Investigation of competitive recombination processes in rare-earth activated garnet phosphors

D. J. Robbins, B. Cockayne, B. Lent, C. N. Duckworth, and J. L. Glasper
Royal Signals and Radar Establishment, Great Malvern, Worcestershire, England
(Received 16 July 1976; revised manuscript received 2 June 1977)

Spectral, kinetic, and relative quantum intensity measurements are reported for a series of $Y_3Al_5O_{12}$ (YAlG) crystals, both nominally undoped and activated by Ce^{3+} and Tb^{3+} The undoped crystal shows a complex emission band in the near uv with fast- and slow-decaying components, analogous to the alkali halides. The band shape appears to involve emission from an unrelaxed and a relaxed defect state of the lattice. In the doped crystals these defect states compete with the activator ions as recombination pathways. The essential properties of the rare-earth activated crystals are described by a simple kinetic model, and initial estimates of the relative magnitudes of the rate constants are made. Temperature-dependence measurements for the cathodoluminescence of the YAlG:Ce (0.01%) crystal show that energy trapped at the defect centers can be thermally released, leading to an interaction between the defects and the activator ions. The effective activation energy for release is approximately 1900 cm^{-1} and an initial estimate for the thermalization time constant based on the kinetic model is approximately 160 nsec at room temperature. At low concentration the time constant for the initial defect trapping state is slower than this value because of multiple capture effects, $\tau(D) \sim 200$ nsec. The rise and decay curves for Ce^{3+} luminescence reflect this slow time constant, but annealing the crystals in an oxidizing atmosphere introduces an additional shunt path which reduces the luminescence efficiency but decreases the activator time constant to the intrinsic Ce^{3+} value $\tau(Ce) \sim 60$ nsec. The significance of the results for phosphor action in these oxides is discussed.

INTRODUCTION

Recent years have seen rare-earth (RE) ions achieve considerable commercial importance in laser and phosphor applications as the luminescent activators for insulating host lattices. Their use in laser systems generally involves excitation and energy conversion within the localized electronic states of the activator center itself, but there are many applications, for example in the phosphor screens for cathode-ray tubes and for x-ray radiography, which involve excitation at energies above the absorption edge of the host lattice. Since the RE activator ion is usually present only in low concentration, the density of available states dictates that this high-energy excitation be absorbed primarily by the atoms of the host lattice, and degraded within the lattice states until an energy is reached at which the energy conversion processes are no longer dominated by the density of states within the lattice band structure. This energy would reasonably correspond to the energy gap of the host lattice, and it is at this point that energy transfer between lattice and activator becomes most probable, leading ultimately to some radiative recombination within the localized activator states.

If one is to understand the overall mechanism of such a phosphor system it is simplest to separate the whole process into a sequence of events. The general principles governing the final stage of the energy conversion, that of radiative and nonradiative recombination within the shielded $4f$ electron shell of the RE ion, are now fairly well understood. There have also been several approaches to the calculation of the radiation ionization yield (RIY) for thermalized carriers resulting from the initial degradation of high-energy excitation within the lattice states. These have included developments of Shockley's theory of secondary ionization in p-n junctions,[1-3] which predicts a dependence of the RIY on band gap, and theories which assume that the plasma frequency represents the basic quantum whereby fast primary and secondary electrons lose energy to the lattice states.[4,5] There has, however, been rather little work aimed at an understanding of the intermediate stage in the overall mechanism, that of energy transfer between the host lattice and the RE activator ion, although this step will be a critical factor in the total efficiency of the phosphor system. This lattice-activator energy transfer must of course be a competitive process, since even in the total absence of deliberately-doped activator the carrier recombination energy will eventually be dissipated by other conversion pathways. It therefore seems reasonable to suppose that maximization of lattice-activator energy transfer and the control of competing recombination pathways are important features in any phosphor optimization procedure.

This work was undertaken in order to investigate the nature of these various competitive re-

combination pathways in a RE-activated oxide phosphor system. Oxides are of particular interest because of the ease of substitution of rare-earth R^{3+} ions at available trivalent cation sites, and because of their resistance to degradation by high-energy electron beams. The YAlG lattice $Y_3Al_5O_{12}$ was selected because good-quality single crystals of this material can now be readily grown, and the activators Ce^{3+} and Tb^{3+} were chosen because of their particular interest in fast scintillator and green visual display systems, respectively.[6] In addition, we have recently reported[7] an emission spectrum characteristic of the undoped YAlG crystals which was assumed to arise from some unidentified lattice defect, and which gave rise to an undesirable afterglow in the otherwise fast response of YAlG:Ce scintillators.[8,9] In this paper we take advantage of the radiative recombination at the defect center in order to investigate the way in which this center competes with the R^{3+} activators for the lattice excitation energy. It will be shown that the cross section of this defect center is large compared with that of RE activators, so that at low RE ion concentration it can dominate the recombination process. The kinetic model to be developed also presents a more detailed picture of the afterglow mechanism in YAlG:Ce phosphors. A schematic energy-level diagram for the materials considered here is shown in Fig. 1.

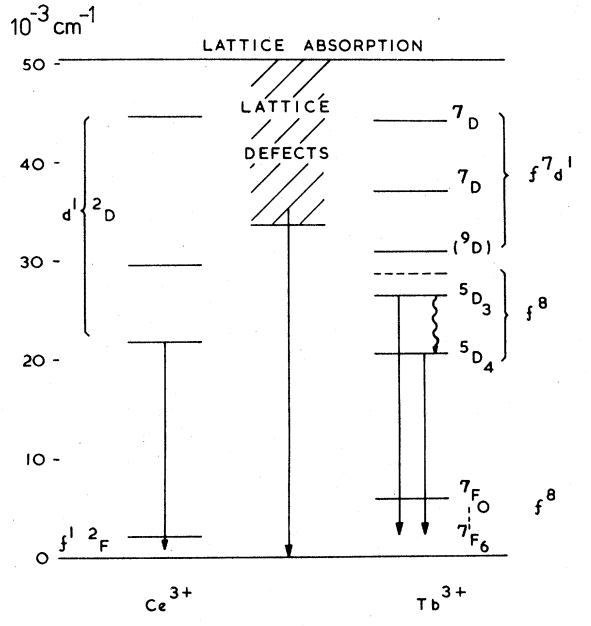

FIG. 1. Schematic diagram of state energies for Ce^{3+} and Tb^{3+} in YAlG. Solid arrows indicate principal emitting states.

EXPERIMENTAL

Crystal preparation

The yttrium aluminium garnet crystals $Y_3Al_5O_{12}:R^{3+}$ (R = Ce, Tb) examined in the present work were all grown by the Czochralski technique using a standard vertical pulling apparatus which has been fully described elsewhere.[10] The melts from which the crystals were grown were prepared in the appropriate molar proportions from the component oxides. The Y_2O_3 was supplied as 99.9999% pure material by Rare Earth Products Ltd., the Al_2O_3 was *BDH* Ltd. Optran grade, the cerium oxide was Specpure quality material from Johnson-Matthey Chemicals Ltd., and the terbium oxide as 99.99% pure material from Rare Earth Products Ltd. The melts were contained in iridium crucibles heated by rf induction under a gas ambient of argon containing 1 vol% oxygen. The crystals were grown using a pulling speed of 1 mm h^{-1} and a crystal rotation rate of 6 rpm. A ⟨111⟩ axis seed was used throughout and slices of 1-mm thickness were cut perpendicular to the growth axis to expose (111) crystal surfaces for luminescence studies. The slices were mechanically polished with successively finer grades of diamond paste with a final polish using SYTON.

Crystal annealing

Absorption and luminescence measurements were made on crystals in the as-grown condition, and after a 48-h anneal in flowing oxygen or hydrogen (100 cm^3 min^{-1}) at 1600 K. The annealing was carried out in a standard Pt-wound resistance furnace in which the samples were raised to temperature over a period of approximately 10 h and furnace cooled over a similar time.

Crystal composition

Melts of different activator concentrations $Y_3Al_5O_{12}:R$ (x%) were prepared according to the following formulas:

$$(Y_{1-x}R_x)_3Al_5O_{12} \quad \begin{matrix} (R=\text{Ce},\ x=0.05,\ 0.5,\ 1.0,\ 2.0,\ 3.0) \\ (R=\text{Tb},\ x=0.1,\ 1.0,\ 3.0,\ 10.0,\ 30.0). \end{matrix}$$

Some (10–20)% of the melt was converted into single crystals and no significant difference in rare-earth activator concentration was found either by x-ray fluorescent analysis (XRFA) or by optical-absorption measurement between slices cut from the top and bottom of each crystal.

The distribution coefficients k_{Ce} and k_{Tb} of Ce and Tb between solid and liquid $Y_3Al_5O_{12}$ were un-

TABLE I. Distribution coefficients for Ce^{3+} and Tb^{3+} ions in YAlG crystals.

Melt composition (No. R atoms per 100 Y atoms)		Crystal composition (XRFA) (No. R per 100 Y atoms)	k_R (XRFA)	k_{Ce} (lattice spacing)
Ce	0.05[a]	...	...	...
	0.05	0.10	0.20	...
	1.0	0.21	0.21	0.18
	2.0	0.25	0.13	0.18
	3.0	0.41	0.14	...
Tb	0.1[a]	...	...	...
	1.0	0.9	0.90	...
	3.0	2.7	0.90	...
	10.0	8.9	0.89	...
	30.0	25.0	0.83	...

[a] R level too low for reproducibility.

known at the outset of the present work, and were estimated using a variety of techniques. XRFA was used to determine the activator concentration in the crystals produced from the melt compositions described above, and the results, given in Table I, suggest that the distribution coefficients vary with composition. This apparent variation was checked by measurement of the integrated optical absorption for the 335- and 456-nm bands of Ce^{3+}, and for the 325-nm band of Tb^{3+}. These showed a linear increase in band area with the melt concentration of Tb^{3+} and a slightly nonlinear increase for Ce^{3+}, indicating that k_{Ce} and k_{Tb} are more nearly constant over the composition range investigated than suggested by XRFA. The variation in the XRFA measurements was particularly marked in the case of Ce, and the validity of the analysis was further tested by comparing very accurate lattice spacings of undoped material with the 1.0%- and 2.0%-Ce samples using the Bond technique.[11] These results, presented in Table II, show a linear increase in lattice spacing with composition which agrees with the integrated optical-absorption data. The lattice spacing changes can also be used to determine the composition change assuming that the Ce substitutes for Y alone in the garnet lattice using the procedure described by Carruthers *et al.*[12] A value of $k_{Ce}=0.18$ was calculated in this way for both the 1.0%- and 2.0%-Ce samples. Hence there is substantial evidence to indicate a smaller variation of k_{Ce} than suggested by the XRFA analysis, but some uncertainty about the absolute value. The values obtained here fall within the ranges

$$k_{Ce}=0.17\pm0.04,$$

$$k_{Tb}=0.88\pm0.05.$$

Throughout the text, however, the activator concentration quoted for a particular crystal will be that obtained by XRFA.

TABLE II. Lattice parameters for undoped and Ce^{3+}-doped YAlG crystals.

Melt composition	Lattice spacing (Å)
$Y_3Al_5O_{12}$	12.00913
$Y_3Al_5O_{12}$(1.0% Ce)	12.00931
$Y_3Al_5O_{12}$(2.0% Ce)	12.00949

Spectral and kinetic measurement

Cathodoluminescence (CL) data were taken on an apparatus constructed in this laboratory and described here for the first time (see Fig. 2). The sample chamber of a Cambridge Instruments Scanning Microanalyzer was modified to accept electrostatic beam deflection plates and a rotating sample holder with associated optics. With no field across the deflection plates the electron beam passed through a 1-mm aperture in a 45° plane mirror on to the sample and light emitted was reflected by the mirror, collimated by a silica lens, passed through a silica vacuum window, and focused on to the entrance slit of a Spex Minimate $\frac{1}{4}$-m monochromator by a second silica lens. The beam could be pulsed away from the mirror aperture with variable mark to space ratio by applying 100-V pulses to one deflection plate, thus enabling kinetic measurements to be made. The switching time could be adjusted to <10 nsec. Gun potential was variable from 5 to 40 kV, and beam current was measured by passing the beam into a Faraday cup in the sample holder, which was insulated from the main body of the instrument.

For measurement of CL spectra the signal from an EMI 9558QB (S20) photomultiplier was taken to

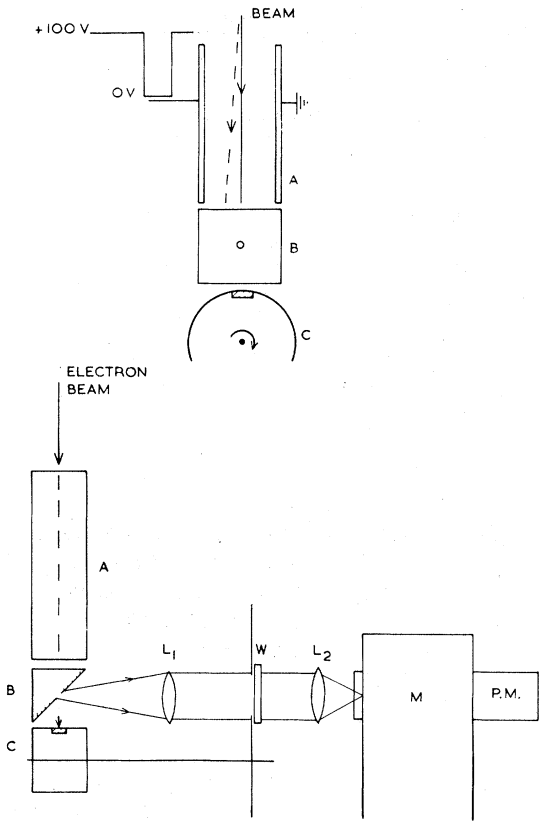

FIG. 2. Demountable cathodoluminescence apparatus. A, electrostatic deflection plates. B, 45° mirror with aperture. C, rotating sample table. L_1, L_2, silica lenses. W, silica vacuum window. M, Monochromator. P.M., photomultiplier.

a Keithley 602 electrometer and the output displayed on a chart recorder. For kinetic measurements the signal from an EMI 9817B fast photomultiplier terminated in a 50-Ω load was fed to a Biomation 8100 fast transient recorder and then to a Nicolet 1072 signal processor. This digital detection system has a maximum time resolution of 10 nsec per point, and allows signal to noise improvement by digital averaging. After a suitable number of sweeps the stored signal was displayed via a Hewlett-Packard 7563A logarithmic amplifier on an X-Y chart recorder. Time-resolved spectra were measured using a Brookdeal boxcar system. Single-crystal samples were mounted by pressing into molten indium on brass discs 8 mm in diameter, and a thin conducting film (e.g., flash-evaporated carbon, or a proprietary aerosol spray) was deposited on the surface to reduce charging effects. Powder samples were ultrasonically dispersed in alcohol, centrifuged onto aluminium discs giving an approximate coverage of 8 mg cm^{-2} and oven dried. The metal discs were attached to the sample holder by high-conductivity silver paint; five samples could be accommodated at any one time. Pulse excitation was used in spectral measurements to reduce the charging problems associated with electron beam measurements on insulators, and no conductive coating was found to be necessary for the powder samples. All spectral data were taken at room temperature and 20-kV beam potential and are not corrected for system response.

The relative emission intensity under cathode-ray (CR) excitation was measured by rotating the sample holder so that the samples were exposed to the beam in sequence. The emitted light was isolated by an appropriate band pass filter and passed directly to the photomultiplier fixed to the vacuum chamber window. In this way each sample was excited under the same conditions and a measure of integrated light output obtained. Relative photoluminescence quantum yields (QY) for the single-crystal materials were measured by attaching the crystals to a small limiting aperture placed at the exit slit of a $\frac{1}{4}$-m monochromator and excited by the monochromated output of a stable deuterium lamp. The emitted light passed through a low-fluorescence cutoff filter to remove the exciting radiation and then through a suitable interference filter directly to the photomultiplier. The crystals were excited over an area larger than the limiting aperture, but since this aperture was smaller than any of the crystals used in the experiment the emission intensity measured by the photomultiplier was not sensitive to refraction effects at the edges of the crystals. Absorption spectra were taken on commercial double beam spectrometers, and were used to correct for the fraction of incident light absorbed by the crystals in the QY measurements. Variable temperature CL measurements were made with a sample on the cold finger of an Oxford Instrument CF100 cryostat fitted with heater and gold-iron vs chromel thermocouple.

RESULTS

Undoped YAlG crystals

The absorption and emission spectra of nominally undoped YAlG crystals in the near uv region are shown in Fig. 3(a). The steeply rising absorption coefficient at ~195 nm marks the onset of the fundamental lattice absorption, but there are weaker absorption bands at lower energy arising from lattice defects. The broad luminescence band peaking at approximately 330 nm has previously been reported[7] and assigned as emission from some unidentified lattice defect. Under high resolution the line spectrum centered at 314 nm shows

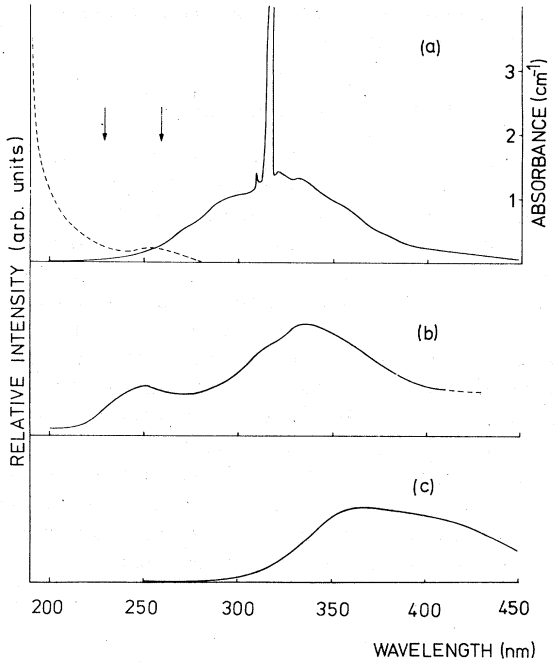

FIG. 3. (a) Absorption (- - -) and CL(——) spectra of nominally undoped YAlG crystal. Arrows indicate near-edge absorption bands. Line emission at 314 nm arises from Gd^{3+} impurity in the component oxide; (b) CL spectrum of Al_2O_3 powder; (c) CL spectrum of Y_2O_3 powder; spectra are not corrected for detector response.

four components with relative intensities determined by the Boltzmann equilibrium[13]; this structure is therefore almost certainly due to the $^6P_{7/2} \rightarrow {}^8S_{7/2}$ transition of Gd^{3+} impurity introduced in the component oxides, the degeneracy of the $^6P_{7/2}$ state being lifted in the D_2 site symmetry to produce four Kramers's doublets.

The broad-band near-uv emission spectrum of YAlG cannot be assigned as the radiative decay of a simple defect center however. Figure 4 shows that the emission can be time-resolved, the peak shifting to lower energy as the signal decays, and a shoulder at approximately 410 nm is found to be more prominent in the spectrum at high excitation densities. Behavior of this kind might be consistent with donor-acceptor pair decay commonly observed in semiconductor materials,[14] or with decay from two or more different centers which have overlapping emission bands. Because of the large shift in peak energy during decay and the increase in intensity at low energy with higher pumping density, we prefer the latter interpretation. There is then a clear analogy to be drawn with the emission spectra of pure alkali halide crystals, many of which show both a high-energy fast-decaying band and a lower energy slow-decaying band.[15] The origin of these transitions is now quite well understood, and they are assigned, respectively, as the radiative recombination of unrelaxed and

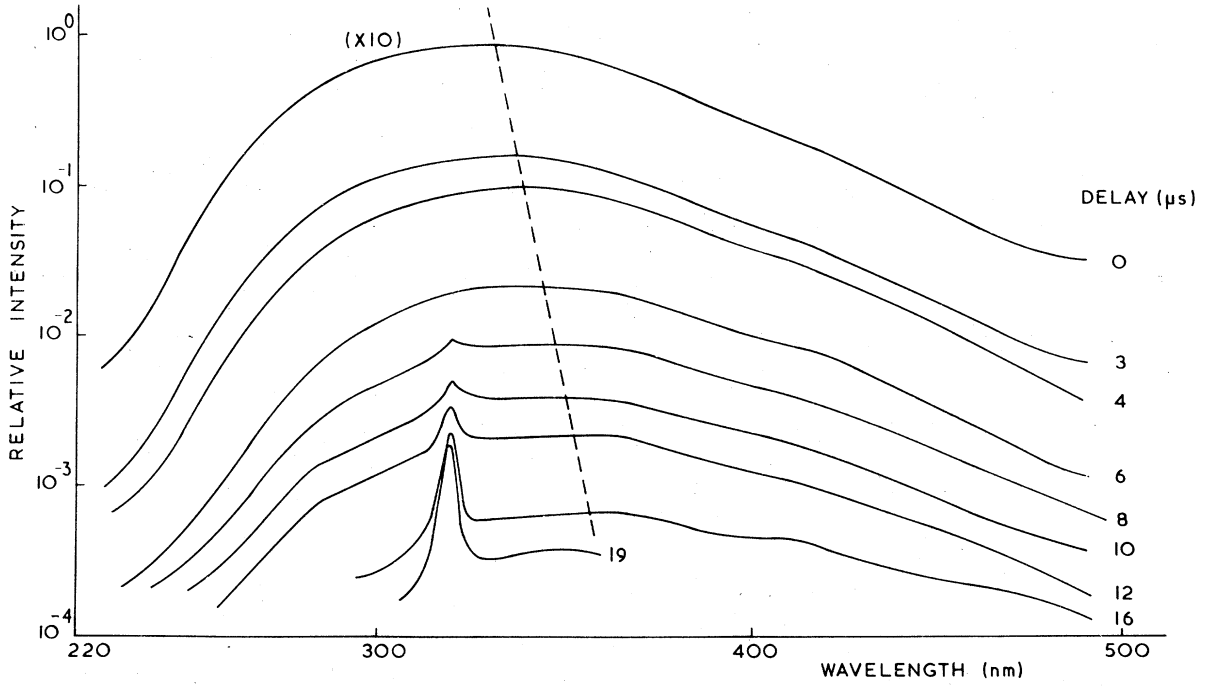

FIG. 4. Time-resolved CL spectra of nominally undoped YAlG. Excitation by 4-μsec electron beam pulse, 1-μsec sampling pulse. The delay is measured between the onset of excitation and sampling pulses.

relaxed exciton states in the ionic alkali halide lattice. The YAlG lattice is also ionic and we tentatively suggest that the broad-band near-uv emission spectrum of YAlG may arise from the overlap of a higher-energy fast-decaying band characteristic of an unrelaxed defect state, and a lower-energy slow-decaying band characteristic of the relaxed defect state. The defect state itself may be associated with an impurity or structural imperfection in the lattice, or may be radiation-induced in a manner similar to the formation of the V_k center or of the self-trapped exciton in alkali halides. Throughout the text we shall refer to this near-uv broad band emission as "defect luminescence" in order to signify that although it is characteristic of the undoped YAlG lattice it is considerably displaced from the lattice absorption edge. For comparison Figs. 3(b) and 3(c) show the near-uv emission spectra of the Al_2O_3 and Y_2O_3 powders used in the crystal growth, and it can be seen that the YAlG spectrum is in some ways intermediate between these two.

Rare-earth activated YAlG crystals

Crystals have been grown with both Ce^{3+} and Tb^{3+} as activator ions, and show the typical activator spectra found in oxide lattices.[6,16] In addition the broad band near-uv emission is still evident in these crystals, but as shown in Fig. 5(a) its intensity decreases rapidly with increasing activator concentration. The data points in Fig. 5(a) are proportional to the relative steady-state concentrations of emitting defects in the various crystals studied, and hence to the net rate for creation of excited defect centers.

The comparison of probabilities for lattice-to-activator energy transfer in Ce^{3+}- and Tb^{3+}- doped crystals is slightly more complicated, however, The relative cathodoluminescence quantum inten-

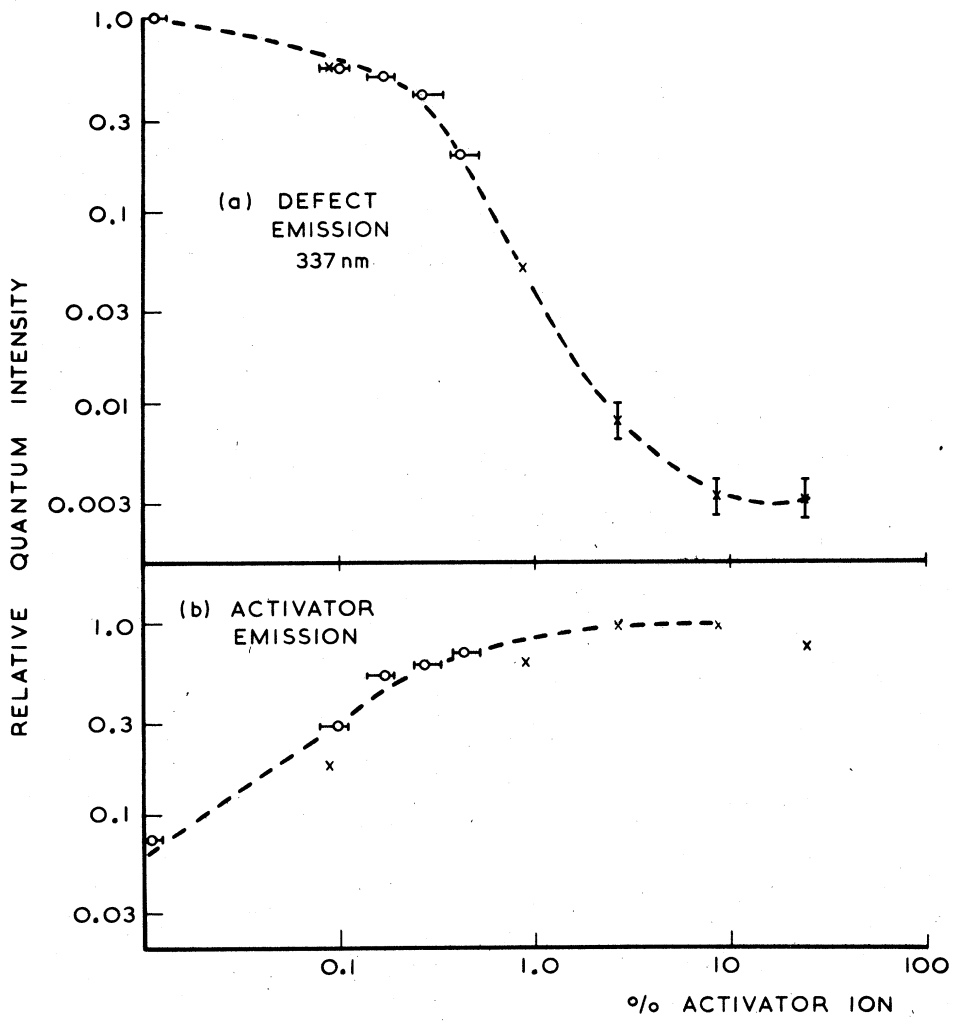

FIG. 5. Relative quantum intensities of emission from (a) lattice defect and (b) RE activator states as a function of activator concentration. Experimental points: ○, Ce^{3+}; ×, Tb^{3+}.

sity (RCLQI) for each activator will be given by the concentration of excited activators times the internal-activator QY. The RCLQI's for Ce^{3+} and Tb^{3+} emission in the series of garnet crystals were determined by comparison of the CL band areas corrected for the detection system response characteristics. The internal-activator QY represents the relative QY for photon emission from excited Ce^{3+} and Tb^{3+} activators once energy transfer from the lattice has occurred. In order to estimate this factor, we assume that energy transfer occurs to those activator states lying just below the lattice absorption edge so that the appropriate activator QY to insert in the above relation is that found by direct optical excitation of the activator states near the absorption edge. The photoluminescence QY's of Ce^{3+} (0.17%) and Tb^{3+} (8.9%) in YAlG for excitation at 235 nm were found to be equal within the experimental error (±10%), so that the internal activator QY was assumed equal for both ions. Hence according to the relation, the RCLQI's are proportional to the steady-state concentrations of excited activator ions and can be used with reasonable confidence to measure tha lattice-activator energy transfer probability under standard excitation conditions. Comparison of intensities in a series of crystals is a valid means for obtaining the relative transfer probabilities since photoluminescence measurements (to be discussed later in connection with annealing studies) show that the quantum efficiency for emission following direct excitation of the activator is reasonably independent of concentration, except for the high concentration YAlG : Tb (25%) crystal. The results of these calculations are shown in Fig. 5(b), where the concentrations derived from XRFA are plotted and the probable error limits suggested by other measurements are indicated. Comparison with a commerical Zn_2SiO_4 : Mn phosphor shows that maximum emitted power in Fig. 5(b) corresponds to a CL energy conversion efficiency of approximately 5%.

It is immediately apparent that the data for the activator ions Ce^{3+} and Tb^{3+} show very similar behavior in both Figs. 5(a) and 5(b), i.e., for any as-grown crystal the intensity of defect luminescence in the near-uv, and the quantum intensity of the activator emission, are largely determined by the general activator concentration in that crystal and are almost independent of whether the activator is Ce^{3+} or Tb^{3+}. It is clear that a decrease in defect emission intensity correlates strongly with an increase in activator emission. This suggests that excitation energy is partitioned between defect and activator centers, the latter dominating at concentrations >1%. Energy exchange might occur directly by long-range resonance transfer from excited defect centers to the activator, or indirectly by thermal release of excitation energy from the excited defect centers into the delocalized lattice states when retrapping at an activator site becomes possible. These alternative models for the defect-activator energy transfer process will be discussed in detail later. In the following section we give further experimental results which have a bearing upon the nature of the interaction between defect and activator centers.

Rise and decay-time measurements

The transfer of excitation between the defect centers and Ce^{3+} has already been recognized as the origin of the afterglow in as-grown YAlG : Ce crystals.[7] The Ce^{3+} ion is a particularly sensitive kinetic probe of these interactions since its intrinsic decay ($\tau_e \sim 60$ nsec at 300 K)[17] is faster than the decay of the defect centers. Figure 6 shows the rise of cathodoluminescence in an as-grown YAlG:Ce (0.1%) crystal in response to a 10-μsec electron beam pulse. The rise of the near-uv defect luminescence is faster at shorter wavelengths, as would be expected if the broad emission band comprises a higher-energy band with short time constant overlapping a lower-energy band with longer time constant. The rise of the Ce^{3+} activator emission in this crystal follows closely the rise of the higher-energy defect emission, and is longer than the intrinsic rise time of Ce^{3+}. Also shown in Fig. 6 is the rise of Ce^{3+}

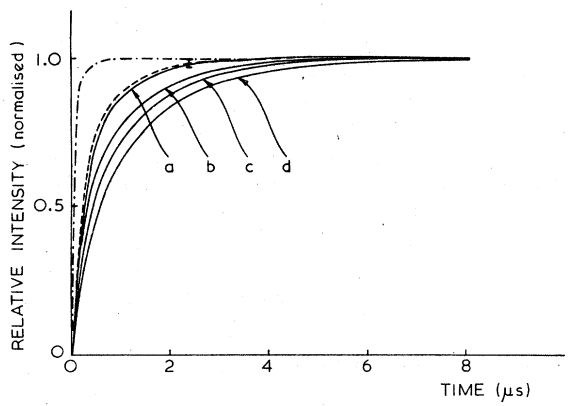

FIG. 6. Rise of CL emission in YAlG:Ce (0.1%) crystals in response to a 10-μsec electron-beam pulse. (——) Defect emission band in an as-grown crystal; (a) 260 nm (b) 280 nm (c) 300 nm (d) 320, 340 nm; (- - -) Ce^{3+} emission at 550 nm in the as-grown crystal; (-·-·-·-) Ce^{3+} emission at 550 nm in an oxygen-annealed crystal. The activator emission follows the shorter-wavelength defect emission in the as-grown material, but is much faster in the annealed crystal. The curves are normalized for comparison.

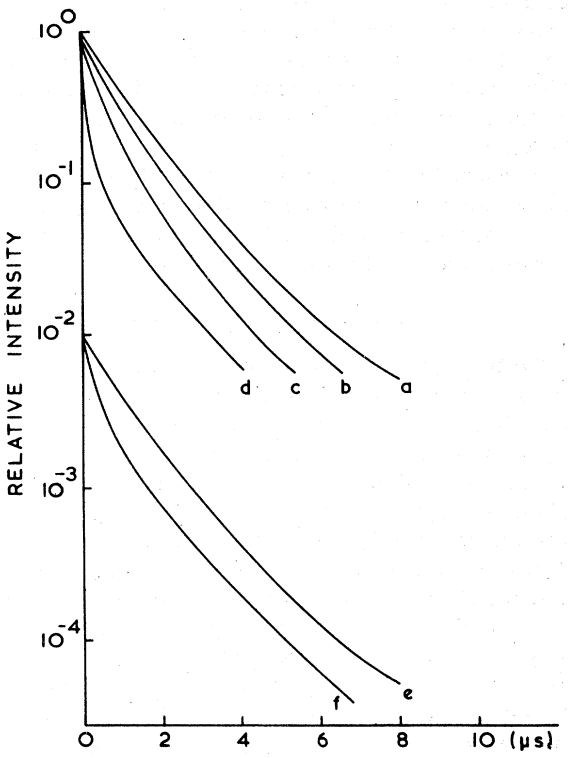

FIG. 7. Decay curves for defect emission at 337 nm. (a) nominally undoped YAlG, as-grown; (b) 0.25% substitution Ce^{3+}; (c) 0.9% substitution Tb^{3+}; (d) 2.7% substitution Tb^{3+}; (e) nominally undoped YAlG, as-grown; (f) nominally undoped YAlG, annealed in oxygen. The curve for the undoped as-grown crystal is given twice [(a) and (e)] in order to show more clearly the effects of activator substitution and annealing on the decay rate.

emission in a slice from the same crystal which had been annealed in an oxygen atmosphere at 1600 K. The rise curve in this annealed crystal is logarithmic with $\tau_e \sim 60$ nsec, close to the intrinsic time-constant of the Ce^{3+} ion. Hence in as-grown YAlG:Ce crystals the kinetics are dominated by the slow time-constants of the defect states; as discussed below, annealing in oxygen reduces the intensity of both defect and Ce^{3+} emission, but eliminates the interaction between defect and activator, so that the activator rise and decay curves are then determined by the intrinsic Ce^{3+} time constant.

In both the direct and indirect energy transfer models outlined above the introduction of activator ions into the crystal effectively generates a new nonradiative recombination pathway for the excited defect centers. This is discussed in detail below. When this occurs, however, we expect the decay rate for defect luminescence to increase as the activator concentration increases, since the energy transfer becomes more probable. Figure 7 shows that this expectation is fulfilled. As in the case of the activator quantum intensities, the increase in defect decay rate apparently depends only on the generalized activator concentration, and is not very sensitive to the chemical differences between Ce^{3+} and Tb^{3+} ions. Qualitatively it is clear from Fig. 7(d) that at high activator concentration (>1%), when the quantum intensity for activator emission approaches saturation, the rate of defect decay to the $1/e$ point is considerably faster than in the nominally undoped YAlG crystal. In this high-concentration limit, the bulk of the lattice excitation energy is ultimately transferred to the activator centers.

It should also be noted that as the concentration of activator increases the excitation initially localized at particular activator sites can migrate amongst the activator centers and eventually be lost at nonradiative sinks.[18] This manifests itself as a significantly nonexponential component in the early part of the $^5D_4$ decay for the YAlG:Tb (25%) crystal, and reduces the apparent transfer QY for this crystal in Fig. 5(b). Concentration quenching then represents a further concentration-dependent factor which would need to be included in any quantitative treatment of activator emission efficiency at very high concentrations. This is not attempted here.

Annealed crystals

Although the experimental data presented above clearly demonstrate that certain defect centers can strongly influence the lattice-activator energy transfer process in garnet crystals, little is known about the nature of the centers themselves. Indeed, as discussed earlier, it is not yet certain whether the defects are radiation-induced and intrinsic to the pure lattice, or are associated with impurities or lattice imperfections. However, the kinetic data for YAlG:Ce crystals indicate that the interaction between defects and activators can be modified by annealing treatment and in this section we report the results of annealing studies on the Ce^{3+}- and Tb^{3+}-doped crystals.

Czochralski-grown garnet single crystals often show colorations which are detrimental to laser performance, the different centers being bleached by annealing in reducing or oxidizing atmospheres.[19,20] We have previously reported the presence of absorption bands in the 200–310-nm range due to unidentified centers in nominally undoped YAlG crystals,[7] and have shown that substitution of Ce^{3+} in the lattice increases the absorbance in this range. Annealing in oxygen increases this near-edge absorbance, the increase for a particular crystal depending upon the con-

TABLE III. Relative CL intensity for garnet crystals. (Relative magnitudes ±25%, significant for particular wavelengths only.)

Emission	%R	As grown	Annealed O_2	Annealed H_2
337 nm (defect)	undoped	100	6	•••
	Ce 0.1	50	<1	•••
	Ce 0.21	45	~1	•••
	Ce 0.25	40	~2	•••
	Tb 0.9	5	4	4
	Tb 2.7	0.8	~0.5	~0.8
	Tb 8.9	a	a	a
530 nm (Ce^{3+})	Ce 0.1	19	2.5	•••
	Ce 0.21	39	4	•••
	Ce 0.25	44	10	•••
544 nm (Tb^{3+})	Tb 0.9	67	62	47
	Tb 2.7	87	36	80
	Tb 8.9	100	87	87

[a]Intensities low but comparable in magnitude.

centration of Ce^{3+} impurity. Absorption measurements on the Tb^{3+} activated crystals show no evidence for a similar dependence of near-edge absorbance on Tb^{3+} concentration, and annealing in oxygen or hydrogen at 1600 K produces little change in the absorption spectra.

The effects of annealing on the relative CL and photoluminescence (PL) quantum yields for the garnet crystals are shown in Tables III and IV. From Table III it can be seen that annealing in oxygen produces a marked decrease in the efficiency of both defect and activator CL emission for the Ce^{3+}-doped crystals, but oxidizing or reducing treatment of the Tb^{3+}-doped crystals produces much smaller effects. The PL data in Table IV show that for direct pumping of the activator transitions (340 nm for Ce^{3+}, 278 nm for Tb^{3+}) the annealing treatments produce relatively small effects, but for pumping at higher energies where both the near-edge absorption and the activator can contribute, the quantum yields are more variable and more sensitive to annealing treatment. This is particularly true of the Ce^{3+}-doped crystals pumped at 260 nm since the near-edge absorption is significant at this wavelength. Hence just as in the case of the absorption spectra, the Ce^{3+}-doped crystals show a much greater sensitivity of their CL and PL quantum yields to an-

TABLE IV. Relative PL quantum yield of RE emission in garnet crystals.[a] (Relative magnitudes significant for a particular wavelength only.)

Excitation	%R	As grown	Annealed O_2	Annealed H_2
340 nm (Ce^{3+})	Ce 0.01	1.12(±0.25)	•••	•••
	Ce 0.1	0.95(±0.1)	0.82(±0.1)	•••
	Ce 0.21	1.0 (±0.05)	0.83(±0.05)	•••
	Ce 0.25	0.97(±0.05)	•••	•••
	Ce 0.41	0.93(±0.05)	0.80(±0.05)	•••
260 nm (defect)	Ce 0.01	•••	•••	•••
	Ce 0.1	0.2 (±0.1)	0.15(±0.1)	•••
	Ce 0.21	1.0 (±0.1)	0.4 (±0.1)	•••
	Ce 0.25	0.7 (±0.1)	•••	•••
	Ce 0.41	1.0 (±0.1)	0.5 (±0.1)	•••
278 nm (Tb^{3+})	Tb 0.9	1.0 (±0.05)	1.0 (±0.05)	1.0 (±0.05)
	Tb 2.7	1.0 (±0.05)	0.9 (±0.05)	1.0 (±0.05)
	Tb 8.9	1.0 (±0.05)	1.0 (±0.05)	1.0 (±0.05)
231 nm (Tb^{3+} + defect)	Tb 0.9	0.9 (±0.05)	0.85(±0.05)	0.95(±0.05)
	Tb 2.7	0.95(±0.05)	0.82(±0.05)	0.97(±0.05)
	Tb 8.9	1.0 (±0.05)	0.95(±0.05)	1.05(±0.05)

[a]Emission wavelength 544 nm for Tb^{3+}, the results being corrected for cross relaxation between $^5D_3$ and $^5D_4$ states.

nealing than do the Tb^{3+}-doped crystals. This possibly arises from the greater mismatch in size between the large Ce^{3+} ion and the Y^{3+} ion for which it substitutes in the garnet lattice.

The large changes in defect emission intensity of the nominally undoped and the Ce^{3+}-doped YAlG crystals at 337 nm following annealing treatment in an oxygen atmosphere are accompanied by an increase in the defect decay rate at this wavelength [Fig. 7(f)]. The change in decay rate however is insufficient to account for the large decrease in intensity and we therefore suggest that the annealing treatment reduces the excitation probability for the emitting state. The decrease in defect emission intensity for the undoped and Ce-doped crystals correlates with the increase in near-edge absorbance in the 200–310-nm region following the oxidizing anneal, and it is tempting to suggest that the decrease in excitation probability at the emitting defect centers is associated with the increased population of absorbing centers, which can act as nonradiative shunt paths. This is more reasonable when it is recalled that the Tb^{3+}-doped crystals show no great sensitivity of either their absorption spectra or their CL quantum yields to the annealing treatments, even when compared with undoped crystal. It appears that the Tb^{3+} substitution in some way stabilizes the garnet crystals against the annealing.

DISCUSSION

The principal experimental observations which establish the relationship between the emitting defect centers and the RE activator ions in the YAlG lattice can be summarized as follows: (i) The defect emission is complex, consisting of overlapping bands which can be time-resolved. (ii) The intensity of near-uv defect emission decreases, and that of the RE ions increases, as activator concentration increases. The relative quantum intensities of defect and activator emission approximate to a $(1-x):\alpha x$ relationship, where α is a constant and x can take the values $0 \rightarrow 1$ nonlinearly as activator concentration increases. (iii) The quantum intensities of Ce^{3+} and Tb^{3+} ions are essentially similar as a function of activator concentration. (iv) The nonradiative decay rate of the defect emission increases with activator concentration. (v) The rise and decay curves of Ce^{3+} in as-grown crystals show slow components typical of the defect state time constants. (vi) For Ce^{3+}-doped crystals annealing in oxygen reduces both defect and activator emission intensity, and the activator emission in annealed crystals has the fast intrinsic Ce^{3+} time constant. Annealing effects on Tb^{3+}-doped crystals are much smaller.

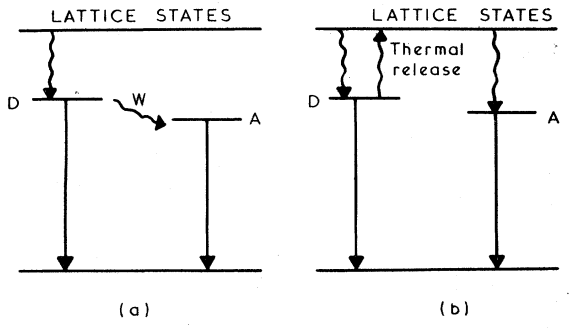

FIG. 8. Two simple kinetic schemes which could give rise to the observed interaction and energy exchange between lattice defect and RE activator states in YAlG. (a) direct through-space long-range resonance transfer; (b) indirect thermalization from defect states with subsequent retrapping at the activator sites.

As pointed out earlier, two simple kinetic schemes would be qualitatively consistent with these observations. The first, illustrated schematically in Fig. 8(a), is the classical direct energy transfer between sensitizer and activator (or donor-acceptor), the archetypal example of this mechanism being the Forster-Dexter long-range resonance transfer (LRRT).[21] In our case the excited defect centers would represent the sensitizers and the RE ions the activator species. The predictions of this model as regards sensitizer and activator quantum efficiency and sensitizer decay characteristics are well known, and are further discussed in the Appendix. There is, however, a second kinetic scheme which is consistent with the experimental data, and which is illustrated in Fig. 8(b). In this case the defect centers can trap the lattice excitation energy, but this energy can then be thermally released from the trapping state and subsequently trapped at an activator ion. As activator concentration increases the probability of multiple capture at the defect states is reduced while the probability of capture at the activator is increased, in accordance with the experimental observations. A practical example of a kinetic scheme analogous to Fig. 8(b) is to be found in the GaP : Zn, O light-emitting diode.[22] There the Zn-O isoelectronic center generates a relatively deep electron trapping state from which thermalization becomes significant around room temperature, reducing the net capture cross-section. In that example, the electron trapping state would be equivalent to the defect and the shunt path for recombination would be equivalent to capture at activator ions in the RE phosphors. Powell and Soos[23] have considered kinetic models for energy transfer in organic molecular crystals which combine aspects

of both kinetic schemes outlined above, but these are only easily solved in the limits represented by Figs. 8(a) and 8(b).

It is qualitatively clear from Fig. 8, however, that we can differentiate between the two schemes by the temperature dependence which they predict for the energy-transfer process. In the sensitizer-activator scheme (a) the energy transfer rate W is expected to be only weakly dependent upon temperature; for LRRT the rate depends upon the overlap of sensitizer fluorescence and activator absorption spectra.[21] Since changes in temperature will probably affect the sensitizer emission intensity via changes in the internal nonradiative recombination processes at the sensitizer center, this model predicts a positive correlation between activator and sensitizer emission intensity with temperature. The thermalization model (b) on the other hand clearly predicts that an increase in temperature will promote thermal release from the state D, reducing the net capture rate at the defect state and increasing the capture probability for the activator A. Hence this model predicts a negative correlation between defect and activator emission, the first decreasing and the second increasing as the temperature is raised.

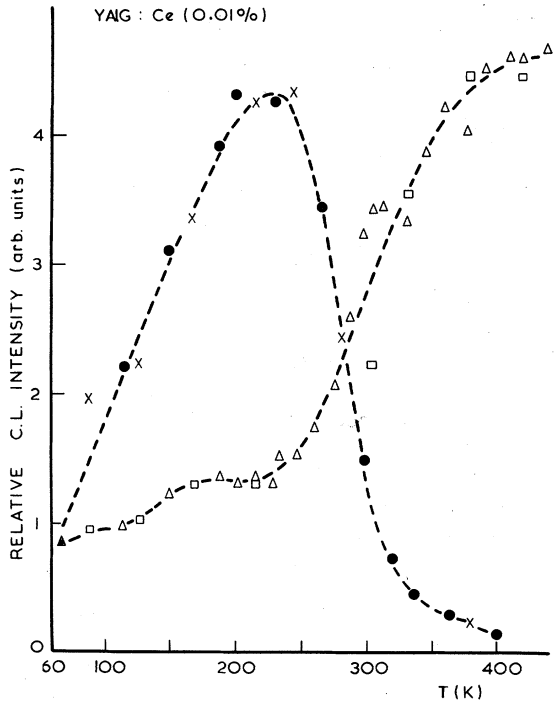

FIG. 9. Temperature dependence of both defect and RE activator CL emission intensity in YAlG:Ce (0.01%). Key to symbols: Defect emission (340 nm): × cooling cycle; • heating cycle. Ce^{3+} emission (550 nm): □ cooling cycle; △ heating cycle. The broken lines connect the experimental points. Note that the intensity of defect emission falls rapidly while that of activiator emission increases at temperatures above 210 K. This is in agreement with the model in Fig. 8(b).

In Fig. 9 is presented the temperature-dependence of the cathodoluminescence intensity for both near-uv defect emission and activator emission in YAlG:Ce (0.01%) in the range 60–440 K. It can be seen that as the temperature increases from 220 to 440 K the intensity of defect emission decreases and that of the activator increases.[24] This is consistent with a model of the type given in Fig. 8(b), in which thermal release from the defect state becomes significant at ~220 K, reducing the net capture rate at the emitting defect centers and thereby reducing the near-uv emission intensity. The thermally released energy, however, becomes available for capture at the Ce^{3+}-ion sites, increasing the activator intensity. It is clear from Fig. 9 that at room temperature the intensity of activator emission in this lightly-doped crystal is limited by competition from the defect centers for the available lattice excitation energy. The effective activation energy for thermal release of energy from the defect states is obtained from the linear region of Fig. 10, and is found to be approximately 1900 cm^{-1}.

From Fig. 3(a) it can be seen that the high-energy side of the near-uv emission band extends to ~210 nm. (The true intensity of this high-energy tail will be larger than shown in the figure since the spectrum is not corrected for the system response which attenuates the signal at increasing energies in this spectral region). It has already been pointed out that the near-uv emission band can be time-resolved into a fast high-energy component and a slower low-energy component. Using the temperature-dependence measurements above we therefore suggest that the fast higher-energy emission band arises from a defect state situated just below the lattice edge, and that this initial trapping state can also undergo a relaxation to a deeper state which has a slower time constant. This relaxation might be compared with the relaxation of the exciton states in alkali halides discussed earlier, which can generate two characteristic lattice emission bands.[15,25] The relaxation of the initial excited defect state in the garnet crystals may involve a spin change analogous to that believed to occur in alkali halides, or may arise from lattice relaxation since the near-uv defect emission band is broad and shows a large Stokes shift, characteristic of strong electron-phonon interaction.

At temperatures below 220 K the changes in activator CL intensity are small, but there is a large decrease in near-uv defect intensity which is not accommodated by the model so far dis-

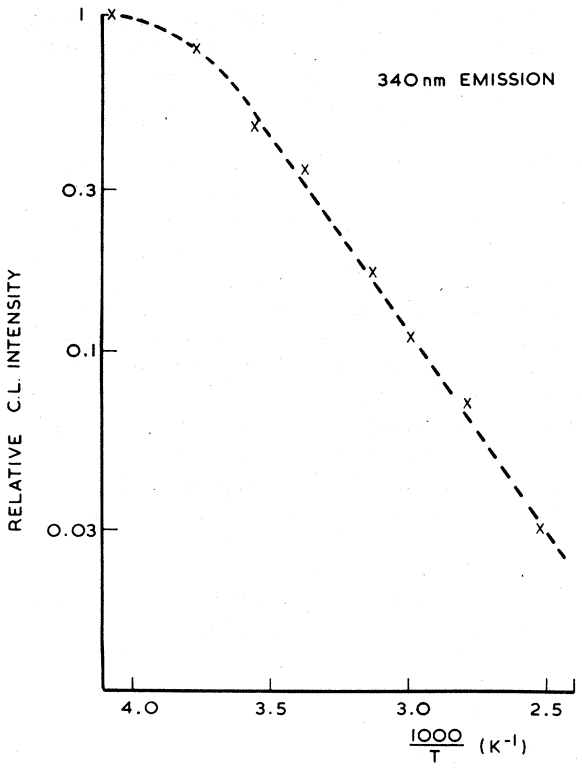

FIG. 10. Semilogarithmic plot of the defect CL intensity data presented in Fig. 9. The exponential region of the curve corresponds to a thermalization activation energy of approximately 1900 cm^{-1}.

cussed. This might be caused by a thermally-activated energy diffusion in the lattice, analogous to the motion of the self-trapped hole in alkali halides,[26] by thermal release of energy from a shallower trapping state or by a phonon-assisted capture cross-section for the defect center itself.[27] The details of this low-temperature interaction are under investigation, but are not essential to the present discussion. Having eliminated scheme 8(a) however, and concentrating upon the temperature dependence above 200 K, it is now possible to construct a kinetic model which can be used to describe the energy transfer processes in the RE garnet phosphors and the temperature dependence of the emission intensities.

Kinetic model

The essential elements of the above discussion are incorporated schematically in Fig. 11. D and D' represent the unrelaxed and relaxed defect excited states, respectively, and A the excited activator states. Thermalization from A is not considered since the strong multiphonon coupling characteristic of the higher excited states of Ce^{3+} and Tb^{3+} ensures rapid relaxation to the deep lo-

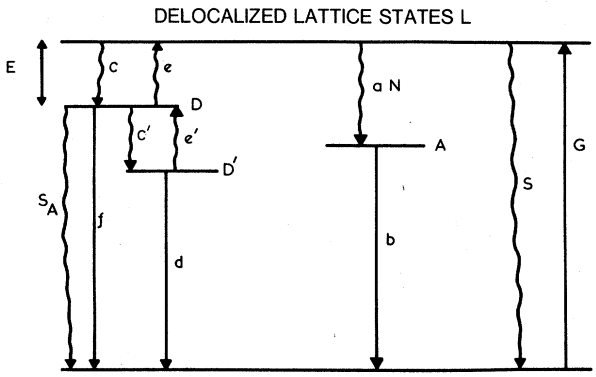

FIG. 11. Kinetic scheme consistent with the experimental measurements relating to energy transfer in rare-earth activated YAlG crystals reported in the text. e and e' represent thermalization rates from the unrelaxed and relaxed defect states D and D', respectively. The thermalization activation energy E is approximately 1900 cm^{-1} in the YAlG:Ce (0.01%) crystal.

calized states of the activator.[28] The nonradiative process S represents an across-gap shunt path, and S_A a shunt mechanism generated by the oxygen annealing in Ce^{3+}-doped crystals, as discussed later. The need for the shunt path S can be seen by comparison of Figs. 9 and 5(b). At high temperatures, the intensity of activator emission in the YAlG:Ce (0.01%) crystal approaches a limit which is approximately twice the room-temperature value, but this still represents only ~13% of the saturation quantum intensity measured at high activator concentrations. The internal quantum efficiency for Ce^{3+} emission is not significantly quenched at 400 K.[17] The intensity of defect emission on the other hand is strongly quenched at this temperature by the thermalization process e, the net creation rate for the defect states becoming small. Since in the YAlG:Ce (0.01%) crystal only ~13% of the available lattice energy finds its way to the activator ions when compared with the high concentration limit it is necessary to postulate the existence of an across-gap shunt path capable of dissipating the energy in the lattice states L.

Assuming low pumping density, the rate equations can then be written

$$\dot{L} = G + eD - (c + aN + S)L\,, \tag{1}$$

$$\dot{D} = cL + e'D' - (e + c' + f + S_A)D\,, \tag{2}$$

$$\dot{D}' = c'D - (e' + d)D'\,, \tag{3}$$

$$\dot{A} = aNL - bA\,. \tag{4}$$

Here G is the pumping rate and N represents the concentration of activator ions. The creation of excited defect centers D is given the unimolecular

rate constant c which assumes that the process has a characteristic rate in as-grown garnet crystals. This characteristic rate could arise because the defect states are radiation induced, or because of a constant concentration of extrinsic defect sites in the as-grown crystals.

In order to determine the relative quantum intensities we take advantage of the fact that the CL measurements were made with 5-μsec pulses, long compared with the time constant of even the slower defect state (see Fig. 7). It is therefore permissible to assume steady-state conditions and solve for L, D, and D' from the equation

$$\dot{L}=\dot{D}=\dot{D}'=0\,. \tag{5}$$

For as-grown crystals $S_A\sim 0$, and initially we assume that the thermalization rate e' from the deep relaxed state D' is negligible. This simplifies the steady-state solution of the rate equations

$$L=G(S+aN+cx)^{-1}\,, \tag{6}$$

$$D=G\{(c'+f)[1+(S+aN/cx)]\}^{-1}\,, \tag{7}$$

$$D'=(c'/d)D\,, \tag{8}$$

$$x=[1+e/(c'+f)]^{-1}\,. \tag{9}$$

In the absence of thermal emission ($e=0$) the rate for creation of excited defect centers D would be c. However thermalization reduces the steady-state net capture rate to cx. At high temperatures, x becomes small so that

$$S+aN\gg cx$$

and

$$x\sim(c'+f)/e \quad \text{(high temperature)}.$$

In the steady state, we also have the condition

$$e/c=g\exp(-E/kT)\,,$$

where g is a degeneracy factor. With these approximations the steady-state concentration of excited defect states D at high temperature can be written in the form

$$D\sim Gc/(S+aN)e\ \sim \text{const.}\times\exp(E/kT)\,, \tag{10}$$

where it is assumed that the temperature dependence of the other rate constants is negligible. This predicted exponential behavior of near-uv defect emission intensity at high temperatures is consistent with the experimental data in Fig. 10, and allows an effective activation energy for the state D to be derived as discussed earlier.

The number of quanta of excitation transferred to the activator in a pulse of length t is given by $aNLt$. The quantum intensity of the activator for fixed excitation pulse length then has the form

$$QI(A)\propto aNG/(S+aN+cx)\,. \tag{11}$$

The limiting behavior of this quantum-intensity curve will be

$$QI(A)\propto aN \quad (\text{low concentration},\ aN\ll S+cx)\,, \tag{12}$$

$$QI(A)\propto \text{constant} \quad (\text{high concentration},\ aN\gg S+cx)\,. \tag{13}$$

It is also possible to make rough quantitative estimates for the relative magnitudes of the various rate constants from the experimental data. We assume that the saturation in quantum intensity at high activator concentration in Fig. 5(b) corresponds to the condition $aN\gg S+cx$, and set this limiting intensity equal to unity. At the high-temperature limit in Fig. 9 we have $x\sim 0$, so that from the earlier discussion we can write, for the YAlG:Ce (0.01%) crystal

$$A_0\sim aN/(S+aN)\sim 0.13 \quad (\text{high temperature},\ x\sim 0)\,. \tag{14}$$

Hence for this crystal $S/aN\sim 7$. At low temperatures, on the other hand, $x\to 1$, so that

$$A_1\sim aN/(S+aN+c) \quad (\text{low temperature},\ x\sim 1)\,. \tag{15}$$

Again for the YAlG:Ce (0.01%) crystal, using the activator intensity at 200 K as the lower limit in Fig. 9,

$$A_0/A_1\sim(S+aN+c)/(S+aN)\sim 3.6\,. \tag{16}$$

Using the previous result for the ratio S/aN, we have $c/aN\sim 21$ for YAlG:Ce (0.01%). At room temperature for this crystal, however, we know

$$A_{RT}\sim\frac{aN}{S+aN+cx}\sim 0.075 \quad (N\equiv 0.01\%)\,. \tag{17}$$

Hence, it is possible to deduce that at room temperature $x\sim 0.25$ and from (9) that the ratio $e/(c'+f)\sim 3$ for the as-grown crystals.

Interpretation of the kinetic data depends upon the general solution of the rate equations (1)–(4). If these are simplified as discussed above by neglecting $e'\sim S_A\sim 0$, then any transient solution for the populations $L(t)$ and $D(t)$ from the coupled Eqs. (1) and (2) will involve two exponentials with time constants λ_- (fast) and λ_+ (slow)[23]:

$$\lambda_\pm=-\tfrac{1}{2}(S+aN+c+k)\pm\tfrac{1}{2}[(S+aN+c-k)^2+4ec]^{1/2}\,, \tag{18}$$

$$k=e+c'+f\,. \tag{19}$$

At room temperature, we have already deduced that $e\sim 3(c'+f)\ll c$. Hence $S+aN+c\gg k$, and these rate constants become

$$-\lambda_-\sim S+aN+c\,, \tag{20}$$

$$-\lambda_+ \sim (c'+f)+e(S+aN)/(S+aN+c)\,. \qquad (21)$$

Broadly speaking, λ_- represents the decay constant for the delocalized lattice states L and λ_+ that for the initial defect trapping state D. At the present time, however, it is only possible to draw qualitative conclusions from the experimental data using these results, since the slow afterglow observed in the decay of the Ce^{3+} activator is characteristic of energy transfer from the relaxed state D', suggesting that the thermalization rate e' may not be negligible and that the solutions obtained by neglecting e' can only be fair approximations.

1. Decay of near-uv defect emission

A measurement of the decay at 255 nm from the YAlG:Tb (0.09%) crystal was made in the hope that the observed decay at this wavelength would be dominated by emission from the higher energy unrelaxed defect state D, and hence give a value for the decay constant λ_+. The observed decay was not a simple exponential, but the time to reach the $1/e$ point was approximately 200 nsec. At an activator concentration of (0.09%) it is possible to deduce from the ratios for the rate constants and (21) that $-\lambda_+ \sim 0.8e$, giving at least a crude estimate for $e^{-1} \sim 160$ nsec at room temperature. The observed decay rate for the state D is less than the thermalization rate at low activator concentration because of the possibility of multiple capture in the defect centers.

The decay at 337 nm in the nominally undoped YAlG crystal shows a slow tail characteristic of emission from the relaxed state D' with rate constant $(d+e')$. Hence $|\lambda_-| \gg |\lambda_+| > d$. Quantitative analysis of the decay at 337 nm is difficult because of the overlap of emissions from D and D', but qualitatively it is clear from (21) that $|\lambda_+|$ will increase with increasing activator concentration N. Since the initial decay at 337 nm should be dominated by the faster process with decay constant λ_+, this prediction is in agreement with the data in Fig. 7, where it can be seen that the initial decay rate increases at higher activator concentrations. At sufficiently high concentration when $aN \gg c+S$, we deduce from the ratio $e \sim 3(c'+f)$ and (21) that $|\lambda_+|^{-1} \sim |1.33e|^{-1} \sim 120$ nsec at room temperature. The decay to the $1/e$ point for the YAlG:Tb (2.7%) crystal, given in Fig. 7(d), is ~150 nsec, in reasonable agreement with the theoretical expectation if the initial decay is dominated by the rate $|\lambda_+|$.

2. Rise and decay curves for Ce^{3+} emission

The rise time for Ce^{3+} emission in as-grown YAlG:Ce (0.1%) is approximately 250 nsec (Fig. 6), and follows closely the rise of the short-wavelength defect emission. Similar time constants, in the range 170–270 nsec, have been observed for the initial decay of Ce^{3+} luminescence in a series of as-grown YAlG:Ce crystals[7] and are all longer than the intrinsic Ce^{3+} time constant $\tau_e(Ce) \sim 60$ nsec. These time constants are close to the previous estimate for $|\lambda_+|^{-1} \sim 200$ nsec based on the 255-nm decay of the YAlG:Tb (0.09%) crystal, suggesting that in the as-grown crystals the Ce^{3+} activator kinetics are dominated by the time constant for the defect trapping state D. Qualitatively this dominance by the state D arises because in all the Ce^{3+} activated crystals the activator concentration is relatively low, the higher concentration Ce^{3+}-doped materials not growing in single crystal form. Hence $c > aN$ for the Ce^{3+} activated crystals, and the majority of lattice excitation energy reaches the Ce^{3+} ions after trapping and thermal release from the defect states D.

The slow afterglow in the Ce^{3+} emission from as-grown crystals has the same time constant as the tail of the defect emission measured at 337 nm. This slow tail is characteristic of the relaxed state D' so that the afterglow indicates transfer of energy from this relaxed state to the activator. This probably occurs through a combination of the thermalization pathways with rate constants e' and e indicated in Fig. 11, although it is possible that direct transfer by a Förster-Dexter mechanism might contribute. Further temperature-dependence measurements on the afterglow phenomenon should prove which is the dominant mechanism.

3. Effects of annealing

It can be seen from Table III that annealing the YAlG:Ce crystals in an oxygen atmosphere reduces the intensity of near-uv defect CL emission and produces a somewhat smaller decrease in the intensity of Ce^{3+} emission. The rise and decay times for the activator luminescence are also faster, and approach the intrinsic time constant $\tau_e(Ce) \sim 60$ nsec (see Fig. 6). These results suggest that a nonradiative shunt path for the defect trapping state D has been introduced by the annealing process, and the appearance of this shunt path correlates with that of the near-edge absorption centers in the annealed crystals, as discussed earlier. This shunt path is represented by the rate constant S_A in Fig. 11. Using the steady-state conditions we have the following equations for the annealed crystals, analogous to (7), (11), and (9):

$$D_A \sim \frac{Gcnx_A}{(c'+f+S_A)(cnx_A+S+aN)}\,, \qquad (22)$$

$$A_A \sim \frac{aNG}{b(S+aN+cnx_A)}, \tag{23}$$

$$x_A = \left(1+\frac{e}{c'+f+S_A}\right)^{-1}. \tag{24}$$

Because of the additional shunt path in the annealed crystals the thermalization factor x_A is greater than that in the as-grown crystals [see Eq. (9)]. The final result is a predicted decrease in the intensity of emission from the defect states D and D', and a smaller decrease in activator emission. From (21) we also expect an increase in the rate constant $|\lambda_+|$ following annealing treatment, these effects combining to reduce the slow transfer of energy between trapping states and the activator ions in the annealed crystals so that the Ce^{3+} emission shows the characteristic lifetime $\tau_e(Ce)$ ~ 60 nsec. Hence, at least in a qualitative sense the introduction of the one additional shunt path for the defect state D is sufficient to explain the experimental data.

CONCLUSIONS

As-grown YAlG crystals typically show a complex near-uv emission band, possibly arising from the overlap of emission from an unrelaxed and a relaxed defect state. The defects may be radiation-induced and a property of the pure lattice, similar to the V_k center in alkali halides, or they may be extrinsic in origin. The energy capture rate at the defects is larger than that at the Ce^{3+} or Tb^{3+} activator ions until concentrations approaching 1% are reached; a saturation in the activator quantum intensity occurs at concentrations > 3%. At low concentrations, especially significant for the Ce^{3+}-doped material, activator excitation depends upon transfer of energy from defect trapping centers to the RE ions. Temperature-dependence measurements demonstrate that above 200 K this transfer occurs predominantly via thermal release of energy from the trapping sites rather than by long-range resonance transfer. A simple kinetic model which assigns a concentration independent rate constant to the various processes is shown in Fig. 11 and gives good qualitative agreement with the measured intensity and kinetic data.

An important parameter in the model is the thermalization factor x defined in Eq. (9). If $x \sim 1$, then thermal release of energy from the trapping states is small and the defect centers would act essentially as recombination sites for the lattice excitation energy. Energy transfer would then depend upon LRRT. When $x < 1$ thermalization is significant and the net energy capture rate at the defect centers is reduced from c to cx. At low activator concentration, multiple capture at defect centers is possible, but as activator concentration increases capture at RE ion sites begins to dominate. An initial estimate of the thermalization time constant gives $|e|^{-1} \sim 160$ nsec at room temperature, and $x \sim 0.25$ for YAlG. More quantitative application of the model requires accurate measurement of the rate constants as a function of temperature. This work is now in progress.

Because of multiple energy capture at defect centers, the time constants for initial rise and decay of activator emission in as-grown YAlG:Ce crystals are dominated by the time constant $\tau_e(D) \sim 200$ nsec for the initial defect trapping D. The tail of the Ce^{3+} decay shows a slow afterglow characteristic of the relaxed defect state D'. Annealing these crystals in an oxidizing atmosphere introduces a shunt path for the defect centers which reduces the luminescence efficiency of the crystals but increases the rate of decay to give the characteristic Ce^{3+} lifetime $\tau_e(Ce) \sim 60$ nsec.

Hence at room temperature, thermally activated motion of energy in the garnet lattice is important in determining the quantum intensity and kinetics of activator emission, particularly at low concentration. The energy might be in the form of free carriers or excitons, but these RE-activated oxide systems show a behavior which is formally analogous to that of the Tl-activated alkali-halide scintillators,[26] and to luminescence phenomena in molecular oxide lattices such as $CaWO_4$ where a thermally-activated hopping of self-trapped excitons is believed to occur.[29] The similar concentration dependence of quantum intensity for Ce^{3+} and Tb^{3+} ions suggests that the activator cross-section is not sensitive to the chemical difference between these activators. The factors governing the energy trapping probabilities at different RE ions will be discussed elsewhere.[28]

ACKNOWLEDGMENTS

The authors wish to thank Dr. M. Wise (Center for Materials Science, Birmingham University) for help with x-ray fluorescence analysis, K. H. Lloyd for help with lattice-spacing measurements, D. G. Coates for advice in construction of the CL instrumentation, Dr. P. Greenough for making available the vacuum uv instrumentation at GEC Hirst Research Center, and Dr. P. J. Dean and Dr. D. C. W. Herbert for many helpful discussions.

APPENDIX

LRRT model

The expressions for donor (D) and acceptor (A) quantum yield assuming dipolar interaction are[30]

$$\frac{\eta_D}{\eta_0} = 1 - \left(\frac{\pi}{2}\right)\left(\frac{C_A}{C_0}\right)\exp\left(\frac{\pi(C_A/C_0)^2}{4}\right) \times \left[1 - \operatorname{erf}\left(\frac{\pi^{1/2}C_A}{2C_0}\right)\right], \quad \text{(A1)}$$

$$\frac{\eta_A}{\eta_0} = \left(\frac{1}{B\tau}\right)\left(1 - \frac{\eta_D}{\eta_0}\right), \quad \text{(A2)}$$

where C_A is the activator concentration, C_0 an interaction parameter, τ the decay time and B the radiative rate for an isolated donor center, and η_0 the donor quantum yield in the absence of acceptors. The donor decay curve is given by

$$\overline{\rho}(t) = \exp\left[-\frac{t}{\tau} - \left(\frac{C_A}{C_0}\right)\pi^{1/2}\left(\frac{t}{\tau}\right)^{1/2}\right]. \quad \text{(A3)}$$

This model, schematically represented in Fig. 8(a), predicts the correct qualitative relationship between defect (donor) and activator (acceptor) intensity as a function of activator concentration. It also predicts a nonexponential defect decay curve with a rate which increases with activator concentration, as experimentally observed.

However, the model would only predict the observed temperature dependence for the YAlG:Ce (0.01%) CL intensity if the energy transfer rate W increased dramatically with temperature above 200 K. Such an exponential dependence of LRRT rate, which depends upon overlap of donor emission and activator absorption spectra,[21] would be most unusual. There is in fact an increase with temperature in the intensity of the 340-nm absorption band of Ce^{3+} in YAlG,[31] but there are two reasons why this cannot explain the observed temperature dependence. First, the Ce^{3+} absorption intensity increases from 80 K, whereas the exponential decrease in defect emission intensity begins above 200 K. Secondly, the activator emission intensity in the YAlG:Tb (0.09%) crystal under vacuum uv excitation is found to decrease with decreasing temperature in a way which parallels the behavior of the Ce^{3+} activator,[24] but the absorption spectrum of Tb^{3+} in YAlG shows no temperature dependence similar to that of the Ce^{3+} ion.[31] The thermalization model in Fig. 8(b) is therefore necessary to explain the observed temperature dependence and the similarity between the activators Ce^{3+} and Tb^{3+}.

[1]C. A. Klein, J. Appl. Phys. 39, 2029 (1968).
[2]A. Rothwarf, J. Appl. Phys. 44, 752 (1973).
[3]W. Lehmann, J. Electrochem. Soc. 118, 1164 (1971).
[4]J. D. Kingsley and G. W. Ludwig, J. Electrochem. Soc. 117, 353 (1970).
[5]M. S. Waite, in Electrochemical Society Conference Toronto, 1975 (unpublished).
[6]*Optical Characteristics of CRT Screens*, Joint Electron Device Engineering Council Publication No. 16 (Electronic Industries Association, Washington, D.C., 1975).
[7]D. J. Robbins, B. Cockayne, B. Lent, C. N. Duckworth, and F. Mansfield, in *Proceedings of the Twelfth Rare Earth Research Conference, 1976* (Denver Research Institute, Denver, 1976), p. 1004.
[8]G. Blasse and A. Bril, Appl. Phys. Lett. 11, 53 (1967).
[9]E. F. Gibbons, T. Y. Tien, R. G. Delosh, P. J. Zacmanidas, and H. Stadler, J. Electrochem. Soc. 120, 835 (1973).
[10]B. Cockayne, M. Chesswas, and D. B. Gasson, J. Mater. Sci. 2, 7 (1967).
[11]W. L. Bond, Acta. Crystallogr. 13, 814 (1960).
[12]J. R. Carruthers, M. Kokta, R. L. Barns, and M. Grasso, J. Cryst. Growth 19, 204 (1973).
[13]I. Blenkinsop (private communication).
[14]P. J. Dean, Prog. Solid State Chem. 8, 1 (1973).
[15]I. M. Blair, D. Pooley, and D. Smith, J. Phys. C 5, 1537 (1972).
[16]L. G. Van Uitert, in *Luminescence of Inorganic Solids*, edited by P. Goldberg (Academic, New York, 1966).
[17]M. J. Weber, Solid State Commun. 12, 741 (1973).
[18]J. P. Van der Ziel, L. Kopf, and L. G. Van Uitert, Phys. Rev. B 6, 615 (1972).
[19]J. B. Willis and M. Dixon, J. Cryst. Growth 3–4, 236 (1968).
[20]B. Cockayne and B. Lent, in British Association for Crystal Growth Annual Conference, York, 1973 (unpublished).
[21]See for example, Th. Forster, in *Modern Quantum Chemistry, Part III*, edited by O. Sinanoglu (Academic, New York, 1965), p. 93.
[22]C. H. Henry, R. Z. Bachrach, and N. E. Schumaker, Phys. Rev. B 8, 4761 (1973).
[23]R. C. Powell and Z. G. Soos, Phys. Rev. B 5, 1547 (1972).
[24]A similar behavior with changes in temperature in the range 100–300 K has been observed using vacuum uv excitation at an energy just above the lattice absorption edge; P. Greenough, D. J. Robbins (unpublished).
[25]A. M. Stoneham, J. Phys. C 7, 2476 (1974).
[26]R. G. Kaufman, W. B. Hadley, H. N. Hersh, IEEE Trans. Nucl. Sci. 17 (3), 82 (1970).
[27]C. H. Henry and D. V. Lang, *Proceedings of the Twelfth International Conference on Physics of Semiconductors, 1974* (Teubner, Stuttgart, 1974), p. 411.
[28]D. J. Robbins, B. Cockayne, B. Lent, and J. L. Glasper (unpublished).
[29]M. J. Treadway and R. C. Powell, Phys. Rev. B 11, 862 (1975).
[30]M. Inokuti and F. Hirayama, J. Chem. Phys. 43, 1978 (1965).
[31]D. J. Robbins (unpublished).